

A highly efficient single-photon source based on a quantum dot in a photonic nanowire

Julien Claudon^{1†*}, Joël Bleuse^{1†}, Nitin Singh Malik¹, Maëla Bazin¹, Périne Jaffrennou¹, Niels Gregersen², Christophe Sauvan³, Philippe Lalanne³ and Jean-Michel Gérard¹

The development of efficient solid-state sources of single photons is a major challenge in the context of quantum communication, optical quantum information processing and metrology¹. Such a source must enable the implementation of a stable, single-photon emitter, like a colour centre in diamond^{2–4} or a semiconductor quantum dot^{5–7}. Achieving a high extraction efficiency has long been recognized as a major issue, and both classical solutions⁸ and cavity quantum electrodynamics effects have been applied^{9–12}. We adopt a different approach, based on an InAs quantum dot embedded in a GaAs photonic nanowire with carefully tailored ends¹³. Under optical pumping, we demonstrate a record source efficiency of 0.72, combined with pure single-photon emission. This non-resonant approach also provides broadband spontaneous emission control, thus offering appealing novel opportunities for the development of single-photon sources based on spectrally broad emitters, wavelength-tunable sources or efficient sources of entangled photon pairs.

Efficient solid-state sources of single photons (S4P) conventionally feature a quantum dot (QD) integrated in an optical microcavity. At cryogenic temperatures, QDs display spectrally narrow emission lines compatible with the control of spontaneous emission (SE) based on cavity quantum electrodynamics. The Purcell effect, which arises in high Q-factor and low-volume cavities, dynamically funnels most of the QD SE into a single resonant cavity mode^{9–12,14}. If the far-field emission diagram of this mode is directional, as for pillar microcavities, the QD SE can be efficiently collected by external optics. Recently, a vertical cavity surface-emitting laser (VCSEL)-like source associated with an optimized collection set-up has led to a usable, detected, single-photon flux as high as 4 MHz (ref. 11). However, the efficiency ϵ of the source, defined as the probability of collecting a photon into the first lens of the optical set-up, remains limited to about 0.4 (refs 11,15), in spite of the impressive progress in microcavity figures of merit over recent years^{16,17}. In fact, the far-field emission pattern of high-Q microcavities is very sensitive to fabrication imperfections, which degrade ϵ (ref. 8). Furthermore, this strategy, based on the Purcell effect, is also restricted to quasi-monochromatic emitters and is effective only over the narrow bandwidth of the cavity resonance.

For broadband operation, SE control by a one-dimensional photonic system offers very attractive alternative opportunities, as first shown in the context of ring photonic-wire lasers¹⁸. SE control over a 40 nm bandwidth at 950 nm in a single-mode photonic-crystal waveguide has also been demonstrated as a way to relax the constraints associated with a resonant effect^{19,20}. Similar effects are currently under study with slot waveguides²¹. These designs are well adapted to the integration of a S4P in a photonic integrated

circuit, but the efficient funnelling of the emitted photons into an external optical channel remains a challenge.

In this Letter, we demonstrate an alternative approach based on a vertical semiconductor photonic nanowire, which is better adapted to the efficient collection of light. As detailed in a recent theoretical work¹³, this S4P features an InAs QD embedded in a GaAs photonic nanowire (Fig. 1). Its far-field emission pattern is carefully tailored with an integrated bottom mirror and a top conical taper. This geometry simultaneously meets the criteria of broadband SE control and efficient collection of photons by standard optics, with a predicted $\epsilon > 0.9$ over a remarkable 70 nm broad bandwidth at 950 nm.

The cylindrical photonic nanowire considered in this work is made of a high-refractive-index material ($n = 3.45$), and surrounded by a low-index cladding ($n = 1$). Its diameter d is approximately 10 times smaller than those of micropillar S4Ps ($d = 1–3 \mu\text{m}$)^{14,22}, but larger than the diameter of bottom-up nanowire S4Ps ($d = 10–50 \text{ nm}$)²³. In this intermediate range, a strong confinement of the fundamental guided mode HE_{11} , combined with an efficient screening of the coupling into other modes, leads to very efficient SE control¹³. Both effects are maximal for an emitter having an in-plane dipole and located on the wire axis. Assuming a free-space emitter wavelength $\lambda = 950 \text{ nm}$, the calculated fraction of the emitter SE coupled to HE_{11} reaches $\beta = 0.95$ in an infinite photonic nanowire of optimal diameter $d_{\text{opt}} = 0.22\lambda$. Moreover, β exceeds 0.90 for d/λ in the range 0.20–0.29. Such a tolerance, which relaxes the fabrication constraints, is indicative of broadband SE control.

In a finite cylindrical photonic nanowire, photons reaching the top facet are strongly scattered over a broad angular spectrum and the resulting far-field divergence severely limits the collection efficiency²⁴. Smoothly tapered wires were recently proposed to address this issue²⁵. For a small opening angle α (Fig. 1), this ensures the adiabatic conversion of the HE_{11} mode into a strongly deconfined mode, which presents a narrower, Gaussian far-field emission pattern. At the other end of the photonic nanowire, a specific modal mirror is required to reflect the HE_{11} photons that are emitted towards the substrate. In the present context, broadband reflectivity of a metallic layer is highly desirable. However, to avoid detrimental plasmonic antenna effects at the nanowire–metallic film interface²⁶, we used a metal–dielectric structure made of gold covered with a 11-nm-thick SiO_2 spacer, which presents a theoretical modal reflectivity $|r_m|^2 > 0.91$.

A typical device (see Methods for fabrication details) is shown in Fig. 1b. The GaAs wire is 2.5 μm high, with a diameter of about 200 nm. It features a clean geometry, with a smooth top taper and a neat connection to the bottom mirror. A few ($\sim 5–10$) flat self-assembled InAs QDs with an in-plane dipole are located 80 nm above this mirror.

¹CEA-CNRS-UJF group 'Nanophysique et Semiconducteurs', CEA, INAC, SP2M, F-38054 Grenoble, France, ²DTU Fotonik, Department of Photonics Engineering, Technical University of Denmark, Building 343, DK-2800 Kongens Lyngby, Denmark, ³Laboratoire Charles Fabry de l'Institut d'Optique, CNRS, Université Paris-Sud, Campus Polytechnique, RD 128, 91127 Palaiseau, France; [†]These authors contributed equally to this work. *e-mail: julien.claudon@cea.fr

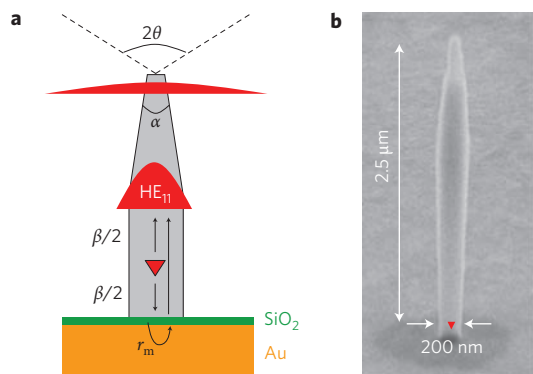


Figure 1 | Single-photon source geometry. **a**, An InAs QD (red triangle) is embedded in a GaAs photonic nanowire. The far-field emission collection is optimized with an integrated modal mirror (gold and SiO₂ spacer) and a smooth tapering of the wire tip (opening angle, α). **b**, Scanning electron microscopy image of a typical device.

Figure 2a shows the micro-photoluminescence (μ PL) spectra of a photonic nanowire S4P in the 911–919 nm wavelength range. The measurements were performed at 5 K, under non-resonant, pulsed optical pumping (see Methods). The spectra exhibit an excitonic line (X) that peaks at 915.2 nm and a bi-excitonic line (XX) peaking at 914.1 nm. Figure 2b shows that their respective integrated intensities I_X and I_{XX} are approximately equal above saturation. This is expected for a single QD with a nearly perfect radiative yield embedded in a source having a broadband collection efficiency. In addition, the nature of these two transitions is unambiguously confirmed by the comparison of these data with the solid curves, calculated from the standard assumption that the probability of creating n excitons in a QD is Poissonian.

The photon statistics of the source were investigated through measurement of the autocorrelation function $g^{(2)}(\tau) = \langle I(t)I(t + \tau) \rangle / \langle I(t) \rangle^2$ under pulsed optical excitation. Above saturation, which corresponds to the maximal source efficiency, the X line exhibits the signature of very pure single-photon emission, with $g^{(2)}(0) < 0.008$ (Fig. 2c). In this regard, photonic nanowires have a key advantage over QD-cavity S4P, which systematically exhibit a much larger $g^{(2)}(0)$ at saturation^{11,15,27}. In a cavity, detuned transitions of the same QD (for example, the XX one) can feed the cavity mode through various mechanisms (dephasing²⁸, coupling to a continuum of states²⁹), which lead to the emission of undesirable multiphoton pulses under non-resonant optical pumping.

The source efficiency ϵ is determined from comparison to a source emitting a known photon flux. To validate the calibration procedure detailed in the Methods, we first investigated a reference S4P, a single InAs QD buried 120 nm under the surface of an unprocessed GaAs sample. With such a simple structure, ϵ is calculated for varying numerical aperture (NA) collection, using an eigenmode expansion technique (solid line in Fig. 3b). At the X saturation, the efficiencies measured with two microscope objectives having NA = 0.4 and 0.75 are respectively $(4.5 \pm 0.8) \times 10^{-3}$ and $(1.2 \pm 0.19) \times 10^{-2}$, in close agreement with theoretical predictions (Fig. 3b).

The same measurements on the X line of the photonic nanowire source with a 0.4 NA first lens lead to $\epsilon = 0.35 \pm 0.05$ (Fig. 3a), very close to state-of-the-art microcavity-based S4Ps (0.44 (ref. 15) and 0.38 (ref. 11)). However, unlike these microcavities, the far-field emission pattern of our photonic nanowires is not fully intercepted by a 0.4 NA collecting cone. Increasing further the collection NA to 0.75 leads to $\epsilon = 0.72 \pm 0.09$, which corresponds to a 55 MHz single-photon flux into the first lens and represents an improvement

by a factor of 1.6 compared to microcavity S4Ps. In addition, we measured several devices with $\epsilon > 0.6$ and reproducibly obtained $\epsilon > 0.5$ on a number of photonic nanowires with diameters ranging from 200 to 260 nm.

The simple Fabry–Perot model developed in ref. 13 provides an analytical expression of ϵ given by

$$\epsilon(\theta) = \frac{1}{2} \beta \frac{(1 + |r_m|)^2}{1 + \beta|r_m|} T_\alpha(\sin \theta) \quad (1)$$

where $T_\alpha(\sin \theta)$ is the taper transmission into free space within a cone of opening angle 2θ . The X decay rate extracted from autocorrelation measurements, equal to 0.42 ns^{-1} , is smaller than the 1 ns^{-1} expected value for an ideal structure. This is likely due to an actual wire diameter $d = 0.9d_{\text{opt}}$, which leads to a deconfinement of HE₁₁. Fortunately, thanks to the strong inhibition of the SE in the other electromagnetic modes, β is robust against imperfections of this kind, and remains about 0.9. In fact, the source efficiency is mainly limited by the upper taper geometry. Our data are well described by a tapering angle $\alpha = 5^\circ$ (solid line in Fig. 3a), leading to $T_{5^\circ}(0.75) = 0.77$. Further fabrication improvement to decrease α may bring the efficiency closer to its theoretical limit, ~ 0.95 for a taper having unity transmission¹³.

Together with a spectacular increase of ϵ , replacing a high-Q cavity design by a monomode waveguide approach comes with another crucial advantage: photonic nanowires offer an intrinsically broadband SE control, applicable to non-monochromatic emitters (colour centres in diamond, QDs operated at higher temperatures). Furthermore, the operating wavelength of the source can be tuned

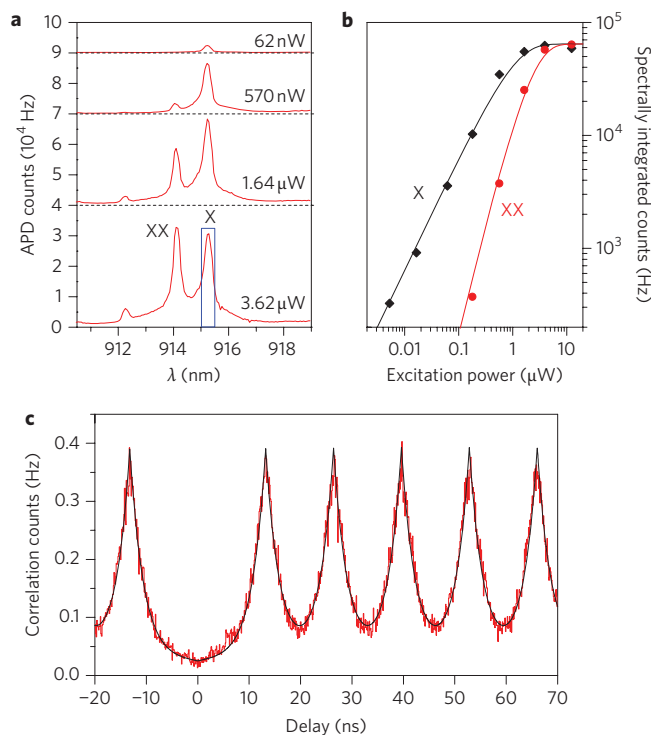


Figure 2 | Single-photon emission by a single QD in a photonic nanowire. **a**, μ PL spectra of the photonic nanowire measured at 5 K for increasing values of the optical pump power P . **b**, Integrated counts of X and XX versus P and fits to the theory (solid lines). Below the saturation pump power $P_0 = 1.05 \mu\text{W}$, they respectively exhibit linear and quadratic dependence on P . **c**, Autocorrelation trace of the X transition (red) well above saturation ($P/P_0 \approx 4$), measured over a 0.5-nm spectral range (rectangle window in **a**). The fit to theory (black) demonstrates $g^{(2)}(0) < 0.008$.

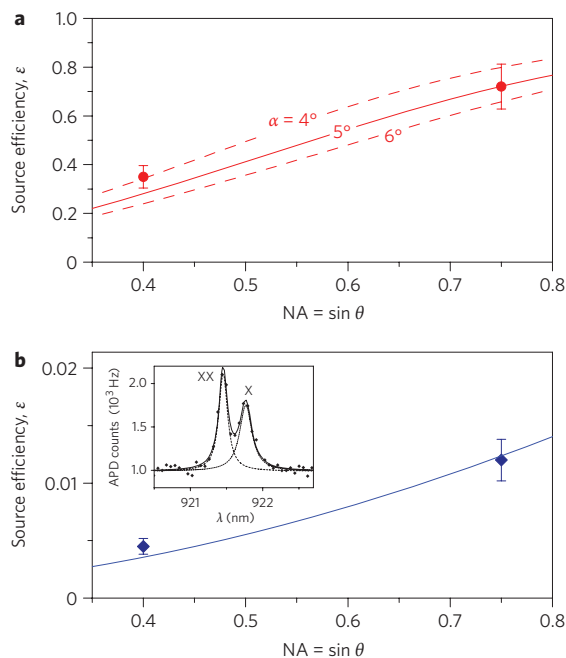


Figure 3 | Efficiency of single-photon sources. **a**, Efficiency of the photonic nanowire source. The measurements (red symbols) were conducted with two microscope objectives ($NA = 0.4$ and 0.75). The three lines are theoretical predictions for three tapering angles α . **b**, Efficiency of the reference source: experimental (blue symbols) and theoretical efficiency (solid line) of a single InAs QD embedded in bulk GaAs, as a function of the first lens NA. The inset shows this QD μ PL spectrum, where both X and XX are saturated. The error bars associated with the measured efficiencies correspond to a 95% confidence interval.

while preserving its efficiency. Finally, the X and XX emission of a single QD can be simultaneously collected to realize an efficient source of entangled photon pairs¹.

On the other hand, the Purcell-based strategy provides an acceleration of the emitter SE rate, which is desirable to increase the source repetition rate or to generate indistinguishable photons¹⁰. Inserting fast emitters in photonic nanowires, such as large InGaAs QD²² or donor impurities³⁰, is thus a natural and appealing perspective of this work.

In conclusion, the photonic nanowire S4P demonstrated in this work combines on-demand, efficient and pure single-photon emission. Moreover, photonic nanowires provide a broadband SE control that increases the device yield. In particular, it opens the way to the realization of room-temperature, efficient S4Ps based on colour centres in diamond, and efficient sources of entangled photon pairs.

Methods

Device fabrication. A planar structure was grown by molecular beam epitaxy. This consisted of an array of Stranski–Krastanov InAs QDs buried in GaAs, 80 nm under the surface. The GaAs layer was 2.5 μ m thick and laid upon a 500-nm-thick $Al_{0.8}Ga_{0.2}As$ sacrificial layer. The composite mirror, consisting of 11 nm of SiO_2 and 250 nm of gold, was then deposited on top of the epitaxial sample. In a flip-chip step, the mirror side of the sample was glued on a GaAs host wafer using epoxy glue. The growth wafer and the sacrificial layer were successively removed by mechanical and selective wet etching, leaving a mirror-flat surface. Finally, after deposition of a 400-nm-thick Si_3N_4 hard mask, an electron-beam lithography step was used to define several identical arrays of aluminium disks of various diameters. After dry etching of the hard mask (SF_6 plasma), the photonic nanowires featuring a top taper were finally defined using carefully optimized plasma etching, used on a $SiCl_4$ and argon gas mixture.

Optical set-up. The samples were mounted in a variable-temperature, helium-flow cryostat. The 820-nm optical excitation was delivered by a 200-fs pulsed Ti:sapphire

laser, with a repetition rate of $f = 76$ MHz. This laser beam was focused down to an ~ 1.5 μ m-diameter spot on the sample with a microscope objective ($NA = 0.40$ or 0.75), which also collected the μ PL signal. Following a 310-mm focal length monochromator, a Hanbury-Brown and Twiss interferometer set-up (detector: silicon avalanche photodiode (APD), time jitter ~ 250 ps) was used to record either the μ PL spectra (summing the detector counts) or the intensity auto correlation function or decay time of the spectrally filtered μ PL.

Source efficiency and set-up detection efficiency. At saturation, the single-photon flux into the first lens emitted by the photonic nanowire was $\phi_X = f\epsilon$. The efficiency ϵ was then obtained from a comparison of ϕ_X with a calibration source: the reflected beam associated with the Ti:sapphire laser, focused on the gold/silica mirror a few micrometres away from the wire, and tuned on the energy $\hbar\omega$ of the X line. The associated photon flux into the first lens was $\phi_{laser} = P_{laser}/\hbar\omega$, where P_{laser} is the measured optical power (in the 50 nW range). We then acquire the spectra of the two sources with the same set-up conditions, except for the use of a density filter (transmission $t = 0.01$) when measuring the reflected laser, to keep the same order of magnitude for the peak APD count rates. The spectrally integrated APD count rates were therefore $I_X = \eta\phi_X$ and $I_{laser} = \eta t\phi_{laser}$, where η is the detection efficiency of the full set-up, and ϵ was then directly deduced from the ratio $I_X/I_{laser} = \phi_X/t\phi_{laser}$. For our set-up, $\eta = 1.2 \times 10^{-3}$ (0.02, optics transmission; 0.2, diffraction grating transmission; 0.3, APD efficiency). This value, comparable to that in ref. 15 ($\eta = 1.1 \times 10^{-3}$), accounts for the magnitude of the detected signals ($I_X \sim 65$ kHz at saturation). Note that before any practical, future use of the source, specific optics should be used to maximize the photon flux in the optical channel of interest (for example, $\eta = 0.13$ in ref. 11).

Received 30 July 2009; accepted 14 December 2009;
published online 31 January 2010

References

- Shields, A. Semiconductor quantum light sources. *Nature Photon.* **1**, 215–223 (2007).
- Brouri, R., Beveratos, A., Poizat, J. P. & Grangier, P. Photon antibunching in the fluorescence of individual color centers in diamond. *Opt. Lett.* **25**, 1294–1296 (2000).
- Kurtsiefer, C., Mayer, S., Zarda, P. & Weinfurter, H. Stable solid-state source of single photons. *Phys. Rev. Lett.* **85**, 290–293 (2000).
- Rabeau, J. R. *et al.* Fabrication of single nickel–nitrogen defects in diamond by chemical vapor deposition. *Appl. Phys. Lett.* **86**, 131926 (2005).
- Gérard, J. M. & Gayral, B. Strong Purcell effect for InAs quantum boxes in three-dimensional solid-state microcavities. *J. Lightwave Technol.* **17**, 2089–2095 (1999).
- Michler, P. *et al.* Quantum correlation among photons from a single quantum dot at room temperature. *Nature* **406**, 968–970 (2000).
- Santori, C., Pelton, M., Solomon, G., Dale, Y. & Yamamoto, Y. Triggered single photons from a quantum dot. *Phys. Rev. Lett.* **86**, 1502–1505 (2001).
- Barnes, W. L. *et al.* Solid-state single photon sources: light collection strategies. *Eur. Phys. J. D* **18**, 197–210 (2002).
- Moreau, E. *et al.* Single-mode solid-state single photon source based on isolated quantum dots in pillar microcavities. *Appl. Phys. Lett.* **79**, 2865–2867 (2001).
- Santori, C., Fattal, D., Vuković, J., Solomon, G. S. & Yamamoto, Y. Indistinguishable photons from a single-photon device. *Nature* **419**, 594–597 (2002).
- Strauf, S. *et al.* High-frequency single-photon source with polarization control. *Nature Photon.* **1**, 704–708 (2007).
- Chang, W. H. *et al.* Efficient single-photon sources based on low-density quantum dots in photonic-crystal nanocavities. *Phys. Rev. Lett.* **96**, 117401 (2006).
- Friedler, I. *et al.* Solid-state single photon sources: the nanowire antenna. *Opt. Express* **17**, 2095–2110 (2009).
- Gérard, J. M. *et al.* Enhanced spontaneous emission by quantum boxes in a monolithic optical microcavity. *Phys. Rev. Lett.* **81**, 1110–1113 (1998).
- Moreau, E. *et al.* A single-mode solid-state source of single photons based on isolated quantum dots in a micropillar. *Physica E* **13**, 418–422 (2002).
- Vahala, K. J. Optical microcavities. *Nature* **423**, 839–846 (2003).
- Noda, S., Fujita, M. & Asano, T. Spontaneous-emission control by photonic crystals and nanocavities. *Nature Photon.* **1**, 449–458 (2009).
- Zhang, J. P. *et al.* Photonic-wire laser. *Phys. Rev. Lett.* **75**, 2678–2681 (1995).
- Lecamp, G., Lalanne, P. & Hugonin, J. P. Very large spontaneous-emission beta factors in photonic-crystal waveguides. *Phys. Rev. Lett.* **99**, 023902 (2007).
- Lund-Hansen, T. *et al.* Experimental realization of highly efficient broadband coupling of single quantum dots to a photonic crystal waveguide. *Phys. Rev. Lett.* **101**, 113903 (2008).
- Jun, Y. C., Briggs, R. M., Atwater, H. A. & Brongersma, M. L. Broadband enhancement of light emission in silicon slot waveguides. *Opt. Express* **17**, 7479–7490 (2009).
- Reithmaier, J. P. *et al.* Strong coupling in a single quantum dot–semiconductor microcavity system. *Nature* **432**, 197–200 (2004).

23. Borgström, M. T., Zwiller, V., Müller, E. & Imamoglu, A. Optically bright quantum dots in single nanowires. *Nano Lett.* **5**, 1439–1443 (2005).
24. Maslov, A. V. & Ning, C. Z. Far-field emission of a semiconductor nanowire laser. *Opt. Lett.* **29**, 572–574 (2004).
25. Gregersen, N., Nielsen, T. R., Claudon, J., Gérard, J. M. & Mørk, J. Controlling the emission profile of a nanowire with a conical taper. *Opt. Lett.* **33**, 1693–1695 (2008).
26. Friedler, I. *et al.* Efficient photonic mirrors for semiconductor nanowires. *Opt. Lett.* **33**, 2635–2637 (2008).
27. Pelton, M. *et al.* Efficient source of single photons: a single quantum dot in a micropost microcavity. *Phys. Rev. Lett.* **89**, 233602 (2002).
28. Suffczynski, J. *et al.* Origin of the optical emission within the cavity mode of coupled quantum dot-cavity systems. *Phys. Rev. Lett.* **103**, 027401 (2009).
29. Winger, M. *et al.* Explanation of photon correlation in the far-off-resonance optical emission from a quantum-dot-cavity system. *Phys. Rev. Lett.* **103**, 207403 (2009).
30. Sanaka, K., Pawlis, A., Ladd, T. D., Lischka, K. & Yamamoto, Y. Indistinguishable photons from independent semiconductor nanostructures. *Phys. Rev. Lett.* **103**, 053601 (2009).

Acknowledgements

The authors acknowledge the pioneering experimental work of R. Hahner and Y.-R. Nowicki-Bringuier, as well as stimulating discussion with I. Friedler, B. Gayral, J.-P. Hugonin, G. Lecamp, J. Mørk and T.R. Nielsen. The work was supported financially by IST-FET European project QPhoton (J.C., J.M.G. and N.G.), 'Nanosciences aux limites de la Nanoélectronique' Fundation (J.C. and N.S.M.), Danish Research Council for Technology and Production (N.G.) and NanoEPR project of the 2006 NanoSci-ERA European program (C.S. and P.L.). Sample fabrication was carried out in the 'Plateforme technologique amont' and CEA LETI MINATEC/DOPT clean rooms.

Author contributions

J.C., N.S.M. and M.B. fabricated the sample. J.B. and P.J. conducted the optical characterizations. N.G., C.S. and P.L. provided theoretical modelling. J.M.G. supervised the project. J.C., J.B. and J.M.G. wrote the paper. All authors commented on the results and the manuscript.

Additional information

The authors declare no competing financial interests. Reprints and permission information is available online at <http://npg.nature.com/reprintsandpermissions/>. Correspondence and requests for materials should be addressed to J.C.